Many-body effects in the mesoscopic x-ray edge problem

Martina Hentschel[1], Georg Röder[1], and Denis Ullmo[2,3]

[1] *Max Planck Institute for Physics of Complex Systems, Nöthnitzer Str. 38, D-01187 Dresden, Germany*
[2] *CNRS, LPTMS UMR 8626, 91405 Orsay Cedex, France*
[3] *Univ. Paris-Sud, 91405 Orsay Cedex, France*

Many-body phenomena, a key interest in the investigation of bulk solid state systems, are studied here in the context of the x-ray edge problem for mesoscopic systems. We investigate the many-body effects associated with the sudden perturbation following the x-ray excitation of a core electron into the conduction band. For small systems with dimensions at the nanoscale we find considerable deviations from the well-understood metallic case where Anderson orthogonality catastrophe and the Mahan-Nozières-DeDominicis response cause characteristic deviations of the photoabsorption cross section from the naive expectation. Whereas the K-edge is typically rounded in metallic systems, we find a slightly peaked K-edge in generic mesoscopic systems with chaotic-coherent electron dynamics. Thus the behavior of the photoabsorption cross section at threshold depends on the system size and is different for the metallic and the mesoscopic case.

§1. Introduction

Many-body phenomena such as the Kondo effect or Fermi edge singularities (FES) have been a key interest in condensed matter physics for many years.[1] Motivated by the experimental progress in the field of mesoscopic physics and quantum chaos,[2] especially the growing interest in many-body effects in those systems,[3] we report here theoretical results on the mesoscopic x-ray edge problem. We are in particular interested in phenomena associated with a sudden perturbation of a mesoscopic system such as a quantum dot or a metallic nanoparticle. We predict substantial differences to the metallic case that are falsifiable in state-of-the-art experiments.

In the x-ray edge problem,[4] a sudden, localized perturbation is caused by an x-ray exciting a core electron into the conduction band, leaving a core hole behind. The response of the conduction electrons to the resulting attractive potential leads to Anderson orthogonality catastrophe (AOC)[5] – the overlap between the unperturbed and perturbed many-body wavefunctions vanishes in the thermodynamic limit. AOC competes with a second many-body effect known as Mahan's exciton[1] or Mahan-Nozières-DeDominicis[6] (MND) response. In the metallic case, this leads to Fermi edge singularities, i.e., deviations from the naively expected photoabsorption cross section in the form of a peaked or rounded edge. More precisely, the behaviour at threshold is known to follow a power law, with the exponent determined by the partial wave phase shifts δ_l at the Fermi energy in response to the sudden perturbation $\hat{V}_c$

for orbital channel l[4] (ω is the x-ray energy, ω_{th} indicates the threshold energy),

$$A(\omega) \propto (\omega - \omega_{\text{th}})^{-2\frac{|\delta_{l_0}|}{\pi} + \sum_l 2(2l+1)\left[\frac{\delta_l}{\pi}\right]^2} . \tag{1·1}$$

The two terms in the exponent have opposite signs and correspond to the MND response (with l_0 being the optically excited channel) and to AOC, respectively.

The many-body enhancement depends, via the dipole selection rules, on the symmetry relation between the core and local conduction electron wavefunction. The MND response will be non-vanishing only if the dipole selection rules are fulfilled. Assuming the local part of the conduction electron wavefunction to be of s-type, we distinguish between core electrons with s-symmetry (K-shell, $l_0 = 1$) and p-symmetry ($L_{2,3}$-shell, $l_0 = 0$)[7] and refer to the photoabsorption threshold as K- or L-edge, respectively. In metals, the phase shifts are such that the K-edge is typically rounded whereas the L-edge is peaked. In the following, we will apply the usual model of a spherically symmetric potential $\hat{V}_c$[4] such that $\delta_l = 0$ for $l > 0$. The origin of the form of the FES typically observed in metals becomes then immediately apparent.[4],[7]

For coherent systems with chaotic or regular dynamics we use a random matrix model[8] or exact solutions of the Schrödinger equation, respectively, to compute the AOC overlap and the photoabsorption cross section. For the latter we use the Fermi golden rule approach introduced by Tanabe and Ohtaka.[4] Our model applies to nanoparticles and quantum dots with chaotic or regular (for example circular) shape, respectively. Comparing our results with the well-understood metallic problem, we find substantial changes:[9],[10] (1) the finite number of particles causes AOC to be incomplete, (2) the sample-to-sample fluctuations of the discrete energy levels produce a distribution of AOC overlaps, and (3) most importantly, the dipole matrix elements connecting the core and conduction electrons are substantially modified. One of our key results is that a photoabsorption cross section showing a rounded edge in metals will change into a slightly peaked edge on average as the size of a chaotic system is reduced to the mesoscopic-coherent scale. This peak is a direct signature of a coherent-chaotic dynamics of the conduction electrons reached in the mesoscopic regime: It is this property that leads to a non-vanishing dipole matrix element[9] and therefore to a situation that is reminiscent of the L-edge behaviour. We will come back to this in more detail below.

The outline of the paper is as follows. First, we consider AOC for mesoscopic systems subject to a sudden, rank-one perturbation. Then, we present results on the photoabsorption cross section in those systems. Our conclusion includes a discussion of possible experimental setups that allow for a verification of our prediction.

§2. Anderson orthogonality catastrophe in mesoscopic systems

We describe the non-interacting system by a Hamiltonian $\hat{H}_0 = \sum_{i,\sigma} \epsilon_i c_{i,\sigma}^{\dagger} c_{i,\sigma}$, where $c_{i,\sigma}^{\dagger}$ creates a particle with spin $\sigma = \pm$ in the orbital $\varphi_i(\mathbf{r})$ ($i = 0, \ldots, N-1$). The unperturbed energy levels ϵ_i are system specific and provide together with the φ_i a unique characterisation of the system. As reference point, we define the *bulklike*

system where the energy levels $\{\epsilon_i\}$ are spaced equidistantly and the wavefunctions are constant.

We furthermore assume that the perturbing potential is a contact potential $\hat{V}_c = \mathcal{V} v_c |\mathbf{r}_c\rangle\langle\mathbf{r}_c|$, with $\mathbf{r}_c$ the location of the core hole and $\mathcal{V}$ the volume in which the electrons are confined. The diagonal form of the perturbed Hamiltonian is $\hat{H} = \hat{H}_0 + \hat{V}_c = \sum_{i,\sigma} \lambda_i \tilde{c}^\dagger_{i,\sigma} \tilde{c}_{i,\sigma}$, where $\tilde{c}^\dagger_{i,\sigma}$ creates a particle in the perturbed orbital $\psi_i(\mathbf{r})$. For relations between the $\{\epsilon_i\}, \{\lambda_i\}$ and $\{\varphi_i\}, \{\psi_i\}$ we refer the reader to Refs.[4), 10)]

A remarkable property of a rank-one perturbation such as a contact potential is that all the quantities of interest for the x-ray edge problem can be expressed in terms of the $\{\epsilon\}$ and $\{\lambda\}$ (or otherwise, for example the wavefunction derivative needed for the dipole matrix element, can be taken as independent random variables following a known, often a Porter-Thomas, distribution). Ignoring for now the spin variable, the overlap between the many body ground states with M particles of $\hat{H}_0$ and $\hat{H}$, $|\Phi_0\rangle$ and $|\Psi_0\rangle$, can be expressed as[4)]

$$|\Delta|^2 = |\langle\Psi_0|\Phi_0\rangle|^2 = \prod_{i=0}^{M-1} \prod_{j=M}^{N-1} \frac{(\lambda_j - \epsilon_i)(\epsilon_j - \lambda_i)}{(\lambda_j - \lambda_i)(\epsilon_j - \epsilon_i)} . \tag{2.1}$$

For the Fermi energy in the middle of the conduction band, the phase shift δ_0, the perturbation strength v_c and the mean level spacing d are related through $\delta_0 = \arctan(\pi v_c/d)$[4)] ($\delta_0$ is negative since the core potential is attractive). In our case, it turns out to be necessary to take boundary effects into account,[10)] which, in addition to the formation of a bound state that is discussed in more detail in Ref.,[10)] modify the phase shifts away from the band center. This can be included simply by introducing a variable v_i given by

$$\frac{1}{v_i} = \frac{1}{v_c} + \frac{1}{d} \ln \frac{N + 0.5 - i}{i + 0.5} .$$

for $i \in (1, N/2)$, and the analogous form for $i \in (N/2, N)$. This gives rise to level-dependent phase shifts δ_i. It is known from the metallic case that the phase shift at the Fermi energy determines the FES. We will now address the question to what extent this statement holds in the mesoscopic case.

In Fig. 1, we first discuss AOC for two mesoscopic systems of different size (with space for N=100 and N=1000 electrons in the conduction band, cf. left and right panels, respectively). The AOC overlap as a function of filling of the conduction band and the perturbation strength is shown in color scale (for reasons of symmetry, we also consider positive v_c in addition to the attractive $v_c < 0$ describing the effect of the core hole). In the top row, the situation in the bulklike case is shown. Clearly, for otherwise equal parameters, the overlap becomes smaller for larger systems (i.e. closer to the thermodynamic limit). There is, however, a considerable amount of structure visible beyond this. The somewhat counterintuitive increase of the overlap with increasing filling is a property of the rank-one model that we use, in particular of the level-dependent phase sifts discussed above. More precisely, within this model the phase shift is, for $v_c < 0$, larger for smaller fillings, see Ref.[10)] for details. In other words, the experimentally relevant phase shift at the Fermi energy depends on
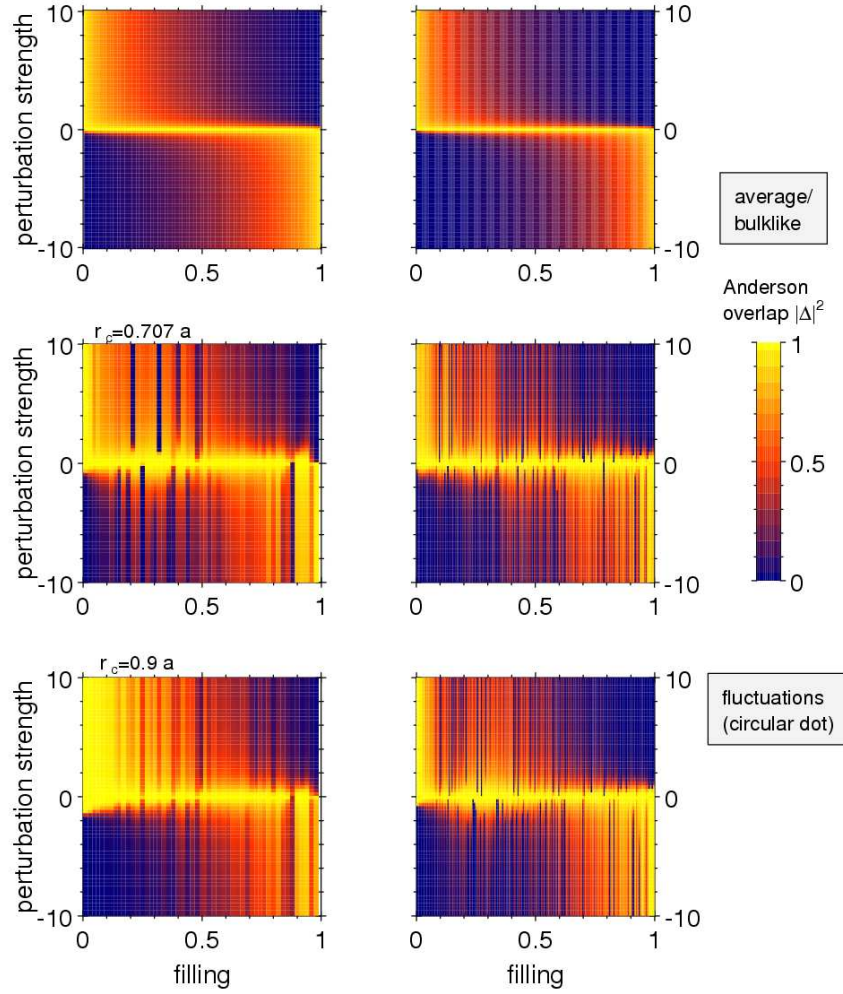
Fig. 1. Anderson orthogonality catastrophe in bulklike systems (top row) and individual mesoscopic systems of different sizes. The larger (smaller) system with space for up to 1000 (100) electrons in the conduction band is shown on the right (left). The mesoscopic system considered here is a circular quantum dot of radius a. The radial position r_c of the perturbation is slightly different in the central and lower row, respectively, giving rise to different behavior of the individual systems.

both the filling and the perturbation strength v_c, and one and the same phase shift can be realized using different sets of parameters, cf. the discussion in the context of Fig. 2 below.

The central and lower row of Fig. 1 show snapshots of some corresponding mesoscopic cases. More specifically, a regular quantum dot of disk shape and with hard walls is considered. To this end, the Schrödinger equation is solved exactly for the energy levels and wavefunctions. The perturbation is placed at two different locations $\mathbf{r}_c$. Fluctuations characteristic for mesoscopic systems are clearly visible. In
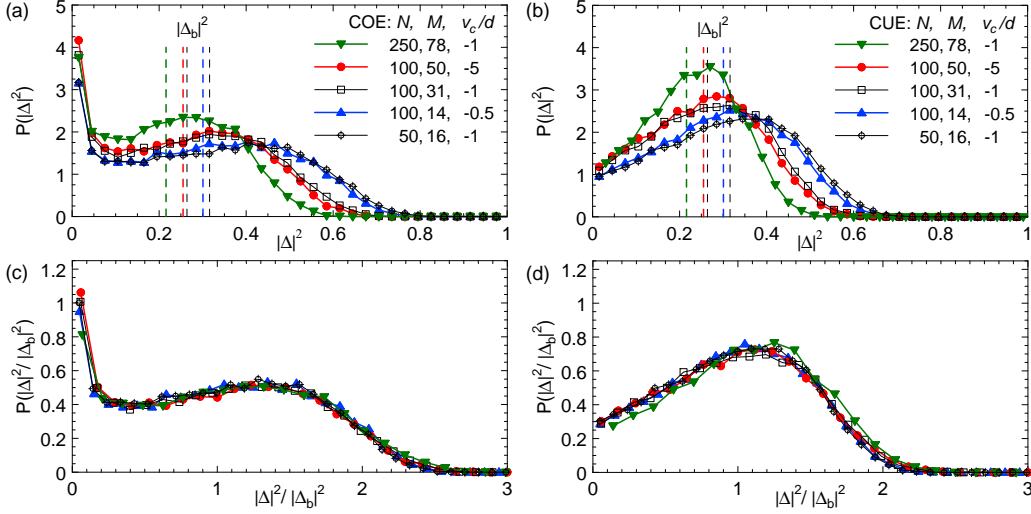
Fig. 2. Distribution of the Anderson overlap $|\Delta|^2$ in chaotic mesoscopic systems. The same phase shift $\delta_F \approx -\pi/2$ at the Fermi energy is realized using different parameter sets $\{N, M, v_c/d\}$ for random matrices from (a) the COE and (b) the CUE ensemble. Once the values $|\Delta|^2$ are scaled by the system-size dependent bulklike overlap $|\Delta_b|^2$, the distributions all coincide: The fluctuations of the overlap depend only on the phase shift δ_F at the Fermi energy.

particular, the overlap is not any more a monotonous function of filling: Changing the filling corresponds to changing the orbital at the Fermi energy. More important than a (model-specific) trend in the phase shift is now the distribution of energy levels around the Fermi energy and the amplitude of the wavefunctions at the position of the perturbation. This also explains the sensitivity of the Anderson overlap against changes of the location of the perturbing potential that are clearly visible when comparing the central and lower row of Fig. 1.

In order to gain a better understanding of the big mesoscopic fluctuations, we will now turn to the universal case of *chaotic* mesoscopic systems, regular systems such a circular quantum dots will be considered elsewhere.[11] We use a random matrix model to effectively describe the (non-interacting) conduction electrons in the absence of the core hole, i.e., we assume the unperturbed energy levels $\{\epsilon_i\}$ to be the eigenvalues of a random matrix (belonging to the circular orthogonal or unitary ensemble,[8] COE or CUE, respectively). The single particle wavefunctions will then show the characteristic Porter-Thomas probability distributions[12] characterizing the spatial dependence of the wavefunction intensity. Ensembles of 10000 individual chaotic systems are generated in a Metropolis algorithm;[10] the joint probability distribution for the $\{\epsilon_i\}$ and $\{\lambda_i\}$, the basic ingredient for this method, was derived in Ref.[13] The Anderson overlap (and later on the photoabsorption cross section) is computed for each realization from Eq. (2·1). Subsequently, average values, probability distributions, etc. are easily determined.

That even in mesoscopic systems the phase shift at the Fermi energy is a physically important quantity as known from the metallic case, becomes clear in Fig. 2. In Fig. 2(a,b), probability distributions of the Anderson overlap are compared for meso-

scopic systems of various sizes possessing time reversal symmetry (COE case, on the left) or not (CUE case on the right). All parameter combinations $\{N, M, v_c/d\}$ yield a very similar phase shift $\delta_F \sim -\pi/2$ at the Fermi energy. Nonetheless, i.e., unlike the expectation based on the behavior of bulk systems would suggest, the probability distributions are rather different. But so are the reference bulklike values for the Anderson overlap indicated by the dashed lines (assignment is such that Δ_b increases in the order of the legend entries). Indeed, the probability distributions for the overlap scaled by the corresponding bulklike value convincingly coincide [lower panels (c) and (d)]: In the mesoscopic case, the overlap does depend on the system size N but the mesoscopic fluctuations are solely determined by the value of the phase shift.

Eventually, we point out the finite probability for finding zero overlap, that moreover is rather different for the COE and CUE case, respectively. Referring the interested reader to the details given in Ref.,[10] the distinctive behavior traces back to the differences of the Porter-Thomas distribution for finding small values in the presence or absence of time-reversal symmetry, respectively.

§3.   Photoabsorption spectra: From rounded to peaked edge

Next, we discuss the absorption spectra, thereby focussing especially on the K-edge. Our approach is based on Fermi's golden rule following the work by K. Ohtaka and Y. Tanabe[4] who showed that this method provides a comprehensive description of the x-ray edge problem. The photoabsorption cross section in the mesoscopic case is then obtained from (using units $\hbar = 1$)

$$A(\omega) = 2\pi \sum_f |\langle \Psi_f | \hat{D} | \Phi_0^c \rangle|^2 \delta(E_f - E_0^c - \omega) , \tag{3.1}$$

where the sum is taken over all perturbed final states Ψ_f (of energy E_f) connected to the unperturbed groundstate $\Phi_0^c = \prod_{\sigma=\pm} \prod_{j=0}^{M-1} c_{j,\sigma}^\dagger c_c^\dagger |0\rangle$ (of energy E_0^c) by the dipole operator $\hat{D}$ ($c_c^\dagger$ creates the core electron in the empty band $|0\rangle$). We are interested in processes involving the core hole; thus, the dipole operator can be written as $\hat{D} = \text{const.} \sum_{j=0}^N \left(w_j \tilde{c}_{j\sigma}^\dagger c_c + h.c. \right)$. At K-edge, the core electron wavefunction and the local part of the conduction electron wavefunction are both of s-symmetry, w_j is related to the *derivative* of the perturbed orbital ψ_j in the direction $\vec{e}$ of the polarization of the x-ray through $w_j = \vec{e} \cdot \nabla \psi_j(\mathbf{r}_c)$.

We first turn to the absorption cross section right at threshold, $\omega = \omega_{\text{th}}$, and neglect the spin degree of freedom for the moment.[1),6)] The only possible final state is then $\Psi_{f0} = \prod_{j=0}^M \tilde{c}_j^\dagger |0\rangle$. Without a perturbing potential, the only contribution is the direct process $w_M \tilde{c}_M^\dagger \tilde{c}_c$. In the presence of a perturbation, however, the new and old orbitals are not identical. This implies that the so-called *replacement processes*, terms with $j < M$, also contribute coherently, giving[4]

$$|\langle \Psi_{f0} | \hat{D} | \Phi_0^c \rangle|^2 \propto |w_M \Delta|^2 \left| 1 - \sum_{i=0}^{M-1} \frac{w_i \Delta_{\bar{i},M}}{w_M \Delta} \right|^2 \tag{3.2}$$

where $\Delta_{\bar{i},M}$ is defined by generalizing Eq. (2·1) with level $i\,(< M)$ replaced by M. Since for chaotic systems the derivative of the wavefunction, $\mathcal{V}k^{-2}\times|\nabla_{\vec{e}}\psi_j|^2$, is known to have Porter-Thomas fluctuations uncorrelated with the wavefunction itself,[14] we can proceed as for the overlap to construct the distribution of $|\langle\Psi_{f^0}|\hat{D}|\Phi_0^c\rangle|^2$.

Away from threshold, part of the x-ray energy can excite additional electrons above the Fermi energy in so-called *shake-up processes*. Their contribution is a straightforward generalization of Eq. (3·2). Although the number of these processes grows in principle exponentially with the energy of the x-ray, only few shake-up processes contribute significantly to the photoabsorption. Shake-up processes involving more than three shake-up pairs can safely be neglected[15] as was also found previously.[16] The spin of the electrons is taken into account by including the AOC contribution due to the additional electronic channel.
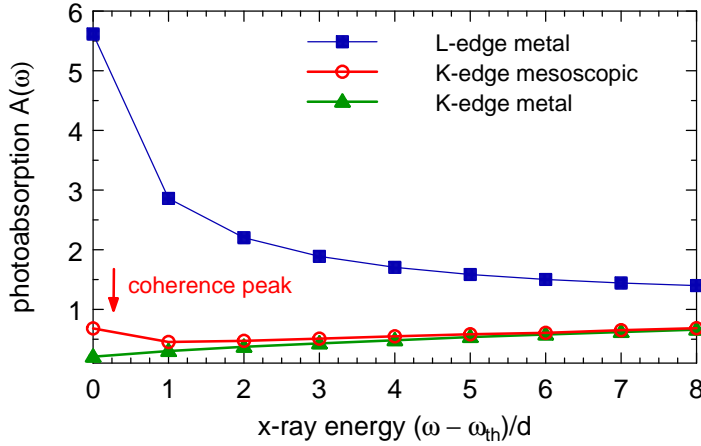

Fig. 3. Photoabsorption spectra for chaotic-coherent mesoscopic systems and bulklike metals in comparison. Whereas the *L*-edge is peaked in both cases, the typically rounded metallic *K*-edge evolves into a peaked signature when the system size is reduced to the chaotic-coherent scale.

The result for the photoabsorption cross section at the *K*-edge of a mesoscopic system is shown in Fig. 3 (open circles). For comparison, the bulklike curves at *K*- and *L*-edge (filled triangles and squares, respectively) are also provided. They are obtained assuming equidistant energy levels and constant dipole matrix elements that explicitly depend on the symmetry relation between the optically active channel and the core electron.[4] As discussed above, this typically leads to a *rounded K-edge* (vanishing dipole matrix elements, only AOC contributes) and a *peaked L-edge* (the MND response, being linear in the phase shift, overcompensates AOC). Remarkably, we find a behavior reminiscent of such a peaked edge at the mesoscopic *K*-edge that is, on average, slightly peaked. This striking difference has its origin in the chaotic-coherent dynamics of the electrons in generic (ballistic) mesoscopic systems such as quantum dots or metallic nanoparticles.

§4. Conclusions

The central result of this work is that changes in the dynamics of electrons in a Fermi sea may imply characteristic changes in the many-body response of the system. They occur, e.g., as a result of a systematic reduction of the system size from the bulklike-metallic to the mesoscopic-coherent scale. One possibility to make these changes visible is through the photoabsorption cross section in response to the sudden creation of a localized perturbation following the excitation of a core electron. In particular, a typically rounded K-edge should develop into a slightly peaked edge when the system size is sufficiently reduced to induce chaotic-coherent dynamics of the electrons. This signature, marked by the arrow in Fig. 3, is an effect of the coherent confinement in the chaotic system where the dipole matrix element at K-edge is determined by the derivative of the wavefunction that, unlike the bulklike case, is independent from the wavefunction itself. Most importantly, it will take non-zero values on average, and consequently lead to a signature that is qualitatively comparable to the metallic L-edge behavior.

Although the effect of the transition to a rounded edge seems to be rather small and requires resolution of the x-ray energy on the order of the mean level spacing (cf. Fig. 3), such an x-ray absorption experiment using metallic nanoparticles should become possible in the near future. Using nowadays technology, we suggest experiments using arrays of quantum dots. The excitation would then not occur by an x-ray and from the core level, but rather by radiation from a microwave laser and from an impurity level specifically introduced by doping in between the valence and conduction band: The physics that we describe here, namely the sudden perturbation of a Fermi sea of electrons by a localized potential, is the very same. The available energy resolution and manageability allow one, in principle, to determine the average values of the photoabsorption cross section and the signature of a coherence peak at the K-edge threshold.

Acknowledgments

References

1) G. D. Mahan, *Many-Particle Physics*, 3rd edition, Kluwer Academic/Plenum Publishers, New York, 2000.
2) L. L. Sohn, G. Schön, and L. P. Kouwenhowen, *Mesoscopic Electron Transport* (Kluwer, Dordrecht, 1997); H.-J. Stöckmann, *Quantum Chaos. An introduction* (Cambridge University Press, Cambridge 1999).
3) I. Hapke-Wurst, U. Zeitler, H. Frahm, A. G. M. Jansen, R. J. Haug, and K. Pierz, Phys. Rev. B. **62**, 12621 (2000); R. O. Vallejos, C. H. Lewenkopf, and Y. Gefen,

Phys. Rev. B **65**, 085309 (2002); Y. Gefen, R. Berkovits, I. V. Lerner, and B. L. Altshuler, Phys. Rev. B **65**, 081106(R) (2002); D. A. Abanin and L. S. Levitov, Phys. Rev. Lett. **93**, 126802 (2004); F. Guinea, Phys. Rev. Lett. **94**, 116804 (2005).

4) K. Ohtaka and Y. Tanabe, *Rev. Mod. Phys.* **62**, 929 (1990) and references therein.
5) P. W. Anderson, Phys. Rev. Lett. **18**, 1049 (1967).
6) B. Roulet, J. Gavoret, and P. Nozières, Phys. Rev. **178**, 1072 (1969); P. Nozières, J. Gavoret, and B. Roulet, Phys. Rev. **178**, 1084 (1969); P. Nozières and C. T. De Dominicis, Phys. Rev. **178**, 1097 (1969).
7) P. H. Citrin, G. K. Wertheim, and M. Schlüter, Phys. Rev. B **20**, 3067 (1979).
8) M. L. Mehta, *Random Matrices,* 2nd edition (Academic Press, San Diego, 1991).
9) M. Hentschel, D. Ullmo, and H.U. Baranger, *Phys. Rev. Lett.* **93**, 176807 (2004).
10) M. Hentschel, D. Ullmo, and H.U. Baranger, *Phys. Rev. B* **72**, 035310 (2005).
11) G. Röder, S. Bandopadhyay, and M. Hentschel, in prep.
12) O. Bohigas, in *Chaos and Quantum Physics* (Les Houches Session LII, 1989), edited by M.-J. Giannoni, A. Voros, and J. Zinn-Justin (North Holland, 1991), pp. 87.
13) I. L. Aleiner and K. A. Matveev, Phys. Rev. Lett. **80**, 814 (1998).
14) V. N. Prigodin, N. Taniguchi, A. Kudrolli, V. Kidambi, and S. Sridhar, Phys. Rev. Lett. **75**, 2392 (1995).
15) M. Hentschel, D. Ullmo, and H.U. Baranger, in prep.
16) J. D. Dow and C. P. Flynn, J. Phys. C: Solid St. Phys. **13**, 1341 (1980).